Applied Surface Science 451 (2018) 250–257

Contents lists available at ScienceDirect

Applied Surface Science

journal homepage: www.elsevier.com/locate/apsusc

Full Length Article

Enhanced performance of perovskite solar cells based on vertical TiO_2 nanotube arrays with full filling of $CH_3NH_3PbI_3$

Xiaoguang Liang [a,d], Yuanhang Cheng [a], Xiuwen Xu [a], Ruoting Dong [a,d], Dapan Li [a,d], Ziyao Zhou [a,d], Renjie Wei [a,d], Guofa Dong [a], Sai-Wing Tsang [a,d], Johnny C. Ho [a,b,c,d,*]

[a] Department of Materials Science and Engineering, City University of Hong Kong, 83 Tat Chee Avenue, Kowloon Tong, Kowloon, Hong Kong
[b] State Key Laboratory of Millimeter Waves, City University of Hong Kong, 83 Tat Chee Avenue, Kowloon Tong, Kowloon, Hong Kong
[c] Centre for Functional Photonics (CFP), City University of Hong Kong, 83 Tat Chee Avenue, Kowloon Tong, Kowloon, Hong Kong
[d] Shenzhen Research Institute, City University of Hong Kong, 518057 Shenzhen, PR China

ARTICLE INFO

Article history:
Received 1 December 2017
Revised 20 April 2018
Accepted 27 April 2018
Available online 30 April 2018

Keywords:
Titanium dioxide (TiO_2)
Nanotube array
Light trapping
Electron transport
Perovskite solar cell

ABSTRACT

Due to a wide range of intriguing properties, such as efficient one-dimensional (1D) electron pathways and extraordinarily large surface areas, titanium dioxide (TiO_2) nanotube arrays are considered as the promising electron transport material for high-performance perovskite solar cells (PVSCs). However, it is still a great challenge to directly synthesize the TiO_2 nanotube arrays with well-controlled geometries (e.g., diameter and height, etc.) on the surface of fluorine-doped tin oxide (FTO). Here, vertically standing TiO_2 nanotube arrays with desirable heights and diameters are directly synthesized on the FTO surface by employing the aqueous TiO_2 sol-gel method on tubular photoresist templates. The tube height can be precisely tailored within a range of 350–900 nm for the effective loading of perovskite precursor solution. Importantly, it is demonstrated that TiO_2 nanotube arrays with the optimized tube diameter and length can facilitate the infiltration of perovskite precursor solution, and thus ensuring the formation of a dense, smooth and large grain-sized perovskite film. Moreover, the contact between the perovskite and TiO_2 nanotube arrays are enhanced simultaneously. Benefiting from the high-quality perovskite film, good interfacial contact at the perovskite/TiO_2 tube interface, enhanced light trapping as well as rapid electron collection and transport induced by one-dimensional TiO_2 nanotubes, the fabricated PVSCs exhibit an impressive power conversion efficiency (*PCE*) of up to 14.13%. Our work does not only demonstrate the promising potential of vertical TiO_2 nanotube arrays for PVSCs, but also provides valuable insights into the design and utilization of TiO_2 nanotubes for practical applications.

1. Introduction

Due to a wide spectrum of extraordinary properties, including the large absorption coefficient, favorable direct band gap, strong defect toleration and excellent carrier diffusion length of >100 nm, solution-processed organometal halide perovskites have attracted enormous attention as the high performance absorber materials for photovoltaic applications [1–5]. Along with the recent intensive research efforts, PVSCs have been experienced with a spectacular progress not only in terms of their power conversion efficiencies but also their optimal device configurations [6–9]. In particular, the mesoporous PVSCs with titanium dioxide (TiO_2) as electron transporting layers (ETLs) have achieved a world recorded efficiency of 22.1%, further highlighting the great potential of utilizing TiO_2 to obtain high-efficiency PSVCs [10]. In any case, although previous works in the field of dye-sensitized solar cells (DSSCs) have already demonstrated that TiO_2 with rationally designed nanostructures can further enhance the device performance [11–13], the utilization of TiO_2 is mainly limited in the form of mesoporous scaffolds for PVSCs [1,10]. More specifically, it is well understood that one-dimensional (1D) TiO_2 nanostructures (e.g., nanorods, nanocones, nanowires, and nanotubes), with the features of efficient one-directional charge transport and extensive loading capacity for the absorber, are considered to be promising ETL candidates [14–17].

Among many of these 1D TiO_2 structures, TiO_2 nanotubes have been triggered with an explosion of research interests for

* Corresponding author at: Department of Materials Science and Engineering, City University of Hong Kong, 83 Tat Chee Avenue, Kowloon Tong, Kowloon, Hong Kong.
E-mail address: johnnyho@cityu.edu.hk (J.C. Ho).

https://doi.org/10.1016/j.apsusc.2018.04.245
0169-4332/

PVSCs owing to their excellent properties of large surface-to-volume ratios, 1D electron diffusion paths, excellent light harvesting capabilities and high surface reactivities [18]. Generally, the synthesis of nanotubes can be accomplished by a variety of methods, namely anodic self-organization processes, hydrothermal methods, template-assisted techniques (e.g., using anodic aluminum oxide, AAO) and others [19–21]. For example, by employing the anodic self-organization methods and in-situ field-assisted chemical dissolution, the fabricated TiO_2 nanotubes based film could be easily harvested from the starting Ti foil matrix after anodization. The obtained nanotubes in the form of macroscopic powders were then dispersed in solution and spin-coated onto the FTO-coated glass to act as ETLs for the subsequent solar cell fabrication [22]. It is noted that these deposited TiO_2 nanotubes were usually oriented in a random manner on the substrate because of their stacking in the solution, leading to the unsatisfied filling of active perovskite materials (e.g., methylammonia iodide, $CH_3NH_3PbI_3$) into the tubes, and thus impairing their unique properties in the efficient electron transport and large surface areas [23]. In order to tackle this issue, a dense Ti layer could be first directly formed on the FTO-coated glass via electron beam deposition, and after anodization, the vertically standing TiO_2 nanotube monolayer was achieved on the transparent substrate with uniform orientation to enable the full filling of $CH_3NH_3PbI_3$ into the tubes [24]. However, since the nanotube diameter and its interspacing between tubes are always relatively small for the anodization fabrication scheme, the full and uniform filling of $CH_3NH_3PbI_3$ into TiO_2 nanotubes becomes somewhat difficult. Even if some tubes can be fully filled, the perovskite crystal sizes are inevitably confined in the range of <30 nm, together with the loose contact between perovskite crystals and nanotube walls, which would eventually degrade the efficiency and the stability of the fabricated devices [24]. At the same time, the incompletely anodized Ti foil might turn into opaque after processing, hindering the effective light absorption for the absorber, and thus resulting in a low photocurrent [25]. On the other hand, the direct growth of TiO_2 nanotubes on electrodes could also be accomplished by using combinations of template-assisted techniques and hydrothermal methods, but the orientation of obtained nanotubes is still arbitrary and cross stacking, destructing their 1D electron diffusion paths [26]. In this regard, it is of great significance to intentionally synthesize TiO_2 tubes with rationally designed nanostructures that can simultaneously ensure the desired perovskite material filling as well as the efficient electron transport.

In our previous work, large-scale and uniform vertical-orientated TiO_2 nanotube arrays with the precisely-controlled diameter, pitch and height have been successfully synthesized on the compact-TiO_2/FTO-coated glass by the enhanced template-assisted method [27–29]. Here, more importantly, these TiO_2 nanotube arrays can be further manipulated with the optimal diameter and height, in which they can be fully and conformally filled by the perovskite material via the simple one-step and solvent-induced method. This way, the fabricated solar cell devices, configured with this dense and smooth perovskite active layer on nanotubes, exhibit the significantly improved power conversion efficiency due to the efficient electron transport and collection as well as the superior light-trapping characteristics. All these results do not only demonstrate the low-cost, facile and direct fabrication of geometry-tunable TiO_2 nanotube arrays on transparent electrodes as the electron transporting layers, leading to a large improvement of photovoltaic performance for PVSCs, but also provide practical utilizations of these TiO_2 nanotube arrays in other solar energy harvesting systems.

2. Experimental section

2.1. Substrate preparation

The vertically standing TiO_2 nanotube arrays with precisely-tuned geometries (i.e., diameter and height) were directly synthesized on the compact-TiO_2 (c-TiO_2)/FTO-coated glass (with the sheet resistance of 10 Ω/sq) according to our previous work [27]. In brief, the FTO-coated glass was rinsed by ultrasonication in succession with deionized (DI) water, acetone and ethanol for 15 min each, followed by a mild oxygen plasma treatment under a process pressure of 0.26 Torr with a power of 30 W for 5 min. Then, a 50-nm-thick compact-TiO_2 layer was formed by spin-coating the titanium isopropoxide (98%, J & K) solution (i.e., 730 μL of titanium isopropoxide diluted in 5 mL of ethanol, and then 2 M, 69 μL of HCl was added to the mixture) onto the FTO surface at 2000 rpm for 60 s. The TiO_2-coated samples were then sintered at 500 °C for 30 min in air.

2.2. TiO_2 nanotube arrays fabrication

The fabricated substrates (c-TiO_2 coated FTO glasses) were first treated with a mild oxygen plasma under 0.26 Torr with a power of 30 W for 5 min. To facilitate subsequent liftoff of the developed photoresist, a 100-nm-thick lift-off resist (LOR 1A) was spin-coated onto the substrate at 4000 rpm for 60 s, and soft-baked at 180 °C for 8 min. Then, photoresist layers with different thicknesses (i.e., 1-μm-thick AZ5214E, 460-nm-thick AZ5206E and 380-nm-thick AZ5206E diluted by an equal volume of 2-propanol) were spin-coated onto the substrates at 4000 rpm for 60 s, respectively, subsequently with a soft-baking at 90 °C for 15 min. After that, polystyrene (PS) nanospheres, 1.28 μm in diameter, were self-assembled on the photoresist film by a Langmuir-Blodgett (LB) method, forming a closely packed monolayer atop. Then, the resulting samples (AZ5214E, AZ5206E, diluted AZ5206E) were subjected to ultraviolet (UV) illumination operated at a flood-exposure mode with a power intensity of 6.5 mW/cm^2 (SUSS MicroTec Mask Aligner, MA/BA6) for 8 s, 4.5 s, and 3.5 s, respectively. After UV irradiation, the PS spheres were removed by DI water ultrasonication, and the exposed samples were developed in AZ-300 MIF developer, followed by the DI water rinsing and nitrogen gas blow dry, successively, to obtain the photoresist templates with tubular holes. In order to ensure complete removal of the residual photoresist at the bottom of holes, all substrates were treated with another mild oxygen plasma at 0.26 Torr with a power of 30 W for 10 s. The resultant photoresist templates were immersed into the aqueous TiO_2 sol-gel solution with a water-to-titanium mole ratio of 200 for 10 s, and then spin-coated at 4000 rpm for 30 s to remove the excessive TiO_2 on top of the photoresist. Next, the vertically oriented TiO_2 nanotube arrays were constructed by dissolving the photoresist templates in ethanol, followed by a 10 min baking (60 °C), DI water rinse and nitrogen blow dry. Finally, the as-constructed TiO_2 nanotube arrays were treated with a 50 mM aqueous $TiCl_4$ (>98%, J&K) solution at 70 °C for 30 min, rinsed with DI water and annealed at 500 °C for 45 min in air to attain the anatase TiO_2 nanotubes. It should be noted that the several nanometers thick of titania thin film connecting the top edges of nanotubes was observed for the thick photoresist samples (AZ5214E), which could be removed by a successive plasma etching under a process Argon pressure of 0.19 Torr with a power of 100 W for 2 min.

2.3. Devices fabrication

For the fabrication of perovskite layers, a simple one-step, solvent-induced and fast crystallization method was employed. In specific, 461 mg of PbI_2, 159 mg of CH_3NH_3I and 79 mg of DMSO

were mixed in 1 mL of DMF solution at room temperature in a glovebox [30,31]. The completely dissolved solution was then dropped onto the planar substrate (c-TiO_2/FTO-coated glass) configured with TiO_2 nanotube arrays with a loading time of 15 s for the tube heights of both 430 nm and 900 nm, followed by spin-coating at 3000 rpm for 30 s. After 6 s of spin-coating, 350 μL of chlorobenzene was quickly dropped onto the center of the rotating substrate. After that, the sample was annealed at 100 °C for 10 min in order to obtain a dense $CH_3NH_3PbI_3$ film. The spiro-MeOTAD (i.e., hole transporting material, HTM) solution was spin-coated onto the deposited perovskite layer at 3000 rpm for 30 s. The HTM solution consists of 36.15 mg of spiro-MeOTAD powder, 14.4 μL of 4-tert-butyl pyridine, 8.75 μL of lithium bis(trifluorome thanesulfonyl)imide in acetonitrile (520 mg/mL) and 500 μL of chlorobenzene. Finally, a 70-nm-thick Au electrode was deposited by thermal evaporation.

2.4. Characterization

The geometrical morphologies of fabricated photoresist templates, TiO_2 nanotube arrays as well as deposited perovskite films were investigated by scanning electron microscopy (SEM, QUANTA FEG450). X-ray diffraction (XRD, SmartLab X-RAY DIFFRACTOMETER, Cu Kα radiation, λ = 1.5406 Å) characterization was also carried out to evaluate the crystallinity of fabricated perovskite films. For TiO_2 nanotubes fully filled with perovskite materials, detailed optical properties were evaluated via ultraviolet-visible (UV–vis) spectrophotometry (Perkin Elmer Lambda 2S UV/VIS Spectrometer). Current-voltage (*I-V*) curves are as well measured under AM 1.5 G (i.e., 1000 W/m^2 at 25 °C) illumination by a solar simulator (Newport Oriel Instruments). The external quantum efficiency (EQE) measurement was conducted by a custom-designed setup consisting of a monochromator, a chopper, a lock-in amplifier (Stanford Research, SR830) and a current preamplifier.

3. Results and discussion

As demonstrated in the previous work, self-assembly of PS nanospheres (1.28 μm in diameter) on top of the photoresist can act as focusing lenses under UV illumination to converge the light profile beneath the spheres [27,29,32]. After removal of PS nanospheres and development of underlying photoresist layers, the highly-ordered tubular photoresist templates with different thicknesses and diameters could be directly deposited onto the rough substrate surface (i.e., c-TiO_2/FTO-coated glass), as illustrated in Fig. 1. In specific, the fabricated templates with controllable tubular thicknesses of 380 and 460 nm were achieved by utilizing the AZ5206E photoresist with and without 2-propanol dilution (Fig. 1a and b). Interestingly, as a result of the tiny difference in their corresponding exposure time of 3.5 and 4.5 s, respectively, the tube diameters of these two templates are very close (i.e., 420 nm and 430 nm). Moreover, by employing the thicker photoresist (AZ5214E), the tubular template with the thickness of 1 μm and the diameter of 650 nm was fabricated under an exposure time of 8 s (Fig. 1c). It is noticed that the AZ5214E template geometry is somewhat different from the ones fabricated by AZ5206E and diluted AZ5206E photoresist. This hexagonal-like feature can be attributed to the longer exposure time and the different propagating nature of UV light in the thicker photoresist, leading to an excessive etching of the AZ5214E template [29]. In this case, various geometrical patterns of the templates can be simply achieved by precise controlling the exposure time and resist thickness. Moreover, since the c-TiO_2/FTO-coated glass substrate consists of a significant surface roughness as well as a uniquely different refractive index as compared with other conventional PV substrates (e.g., Si, pure glass and ITO-coated glass), a 100-nm-thick lift-off resist (LOR 1A) is purposely adopted to spin-coat onto the TiO_2 blocking-layer before the resist deposition, which is found to play a key role in enhancing the uniformity of UV exposure profile in the resist and ensuring the complete resist removal in the subsequent development. These tubular pattern dimensions, including the diameter and the height, can then dictate the geometrical size of subsequently fabricated nanotube arrays.

Next, these tubular photoresist templates were then immersed into the aqueous TiO_2 sol-gel solution, followed by the lift-off of photoresist and the annealing of samples at 500 °C for 45 min in ambient. After that, the vertically oriented TiO_2 nanotube arrays with different diameters and heights, as well as the corresponding morphologies of $CH_3NH_3PbI_3$ deposited onto these nanotubes were obtained, as depicted in Fig. 2. To the best of our knowledge, this is the first report to demonstrate the direct growth of uniform and large-scale TiO_2 nanotube arrays with the well-controlled diameter (410–650 nm) and pitch (1.28 μm) on the rough surface of FTO. After the proper thermal annealing, the anatase phase of TiO_2 tubes could be confirmed by X-ray diffraction (XRD) and Raman spectroscopy as described in the previous report [30]. Fig. 2a–c show the fabricated nanotube arrays with the height and diameter of 350 nm and 410 nm, 430 nm and 430 nm, and 900 nm and 650 nm, respectively, with the same pitch of 1.28 μm. However, as compared with the initial photoresist template thickness, these tube heights got reduced slightly due to the combination of resist

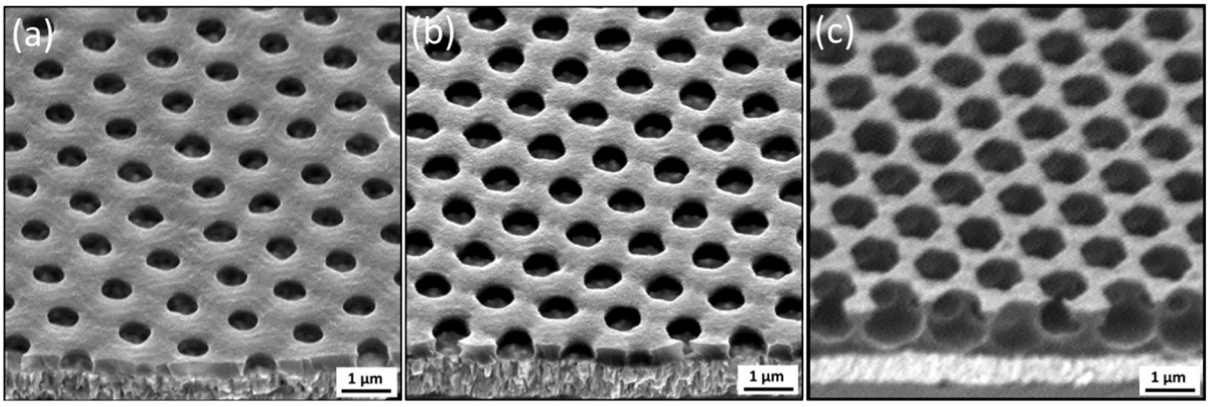

Fig. 1. Scanning electron microscopy (SEM) images of patterned tubular photoresist templates fabricated on the substrates of LOR 1A/c-TiO_2/FTO-coated glass with the pitch of 1.28 μm, the thickness and the hole diameter of (a) 380 nm and 420 nm (AZ5206E diluted by 2-Propanol with the volume ratio of 1 to 1), (b) 460 nm and 430 nm (AZ5206E), and (c) 1 μm and 650 nm (AZ5214).

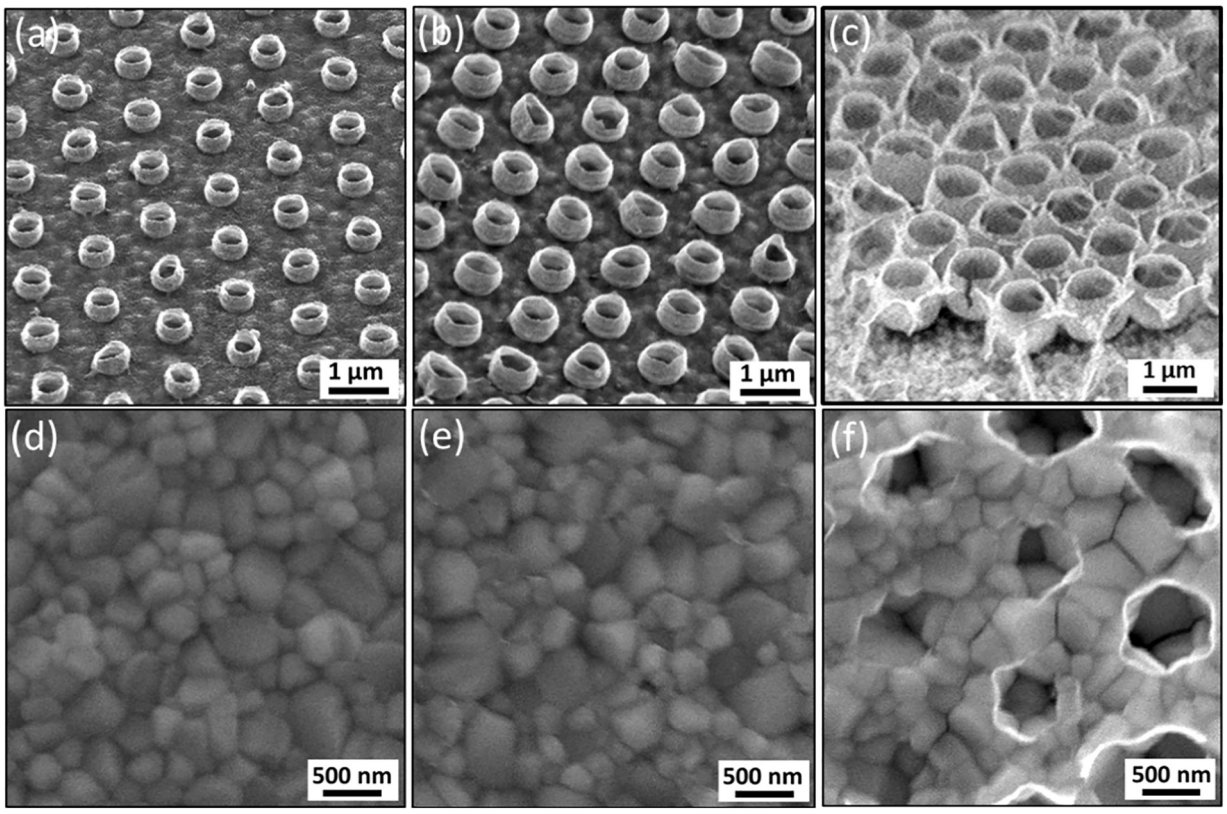

Fig. 2. (a–c) SEM images of TiO_2 nanotubes with the height and the diameter of (a) 350 nm and 410 nm, (b) 430 nm and 430 nm, (c) 900 nm and 650 nm, respectively. (d–f) Top view SEM images of $CH_3NH_3PbI_3$ films spin-coated on different TiO_2 nanotube arrays. (d) The tubes with the height of 350 nm are fully filled and covered by $CH_3NH_3PbI_3$ without the distinct protruding of tube top-edges. (e) The perovskite layer deposited on 430-nm-height tubes formed with a loading time of 15 s. (f) The non-uniform filling of $CH_3NH_3PbI_3$ in 900-nm-height tubes with the loading time of 15 s, where some regions are obviously not filled by the perovskite layer.

lift-off in ethanol, DI water rinse and tube shrinkage during the thermal annealing process. It is also noted that the dimensional uniformity of these nanotubes was not as good as the ones fabricated on conventional substrates, which could be attributed to the irregular UV light distribution in the photoresist induced by the rough surface, leading to the distorted tubular template feature for the tube formation [27]. On the other hand, Fig. 2c presents the TiO_2 nanotubes with a height of 900 nm fabricated via the AZ5214E photoresist template. As discussed above, although there was a residual thin film connecting the top edges of nanotubes fabricated with the thick photoresist template (e.g., AZ5214E), this residual film could be easily removed by plasma etching under a process Argon pressure of 0.19 Torr with a power of 100 W for 2 min. Notably, when the etching time was prolonged, the nanotube height could be further decreased. As a result, considering the tube height manipulation being the main focus of PVSCs studied in this work, a short-time Ar plasma treatment was intentionally performed to remove the residual film without additionally reducing the tube height.

The morphology of perovskite layers deposited on the planar c-TiO_2 and TiO_2 nanotube arrays was then monitored by SEM as shown in Fig. 2d–f and Figs. S1 and S2. It is obvious that the perovskite layer deposited on the TiO_2 nanotube arrays with a height of 350 nm shows a continuous, smooth and compactly-packed film without any pinholes, indicating a desired and uniform filling of perovskite material into the tube arrays (Fig. 2d). Moreover, the grain size of the perovskite crystal, as well as the film morphology, are similar to those deposited on the planar c-TiO_2 as depicted in Fig. S1a. In contrast, when the tube height is increased to 430 nm, a large number of pinholes starts to appear in the perovskite film (Fig. S2a), which is probably due to the insufficient time for infiltration of the perovskite precursor solution. It is well understood that these pinholes introduce short-current pathways and cause direct contact of hole and electron transport materials, which severely deteriorate the device performance. To validate the above hypothesis and simultaneously to achieve the perovskite films with a full coverage, a prolonged loading time is employed for the deposition of perovskite materials. Specifically, prior to the spin-coating, the dropped perovskite precursor solution was maintained on the TiO_2 nanotube arrays for different loading times (e.g., 15 and 30 s), which allows the solution fully infiltrated into the arrays. As anticipated, with 15 s and 30 s loading times, the pinholes of the perovskite film disappeared, as indicated in Fig. S2b and c. The high-magnification SEM image of perovskite film prepared with the 15 s loading time is also presented in Fig. 2e, demonstrating that the tubes are fully and conformally filled by perovskite crystals.

Similarly, Fig. 2f displays the perovskite layer deposited on the 900-nm-height TiO_2 nanotubes with a loading time of 15 s. It is evidently the tubes are not completely filled with the perovskite crystals due to the short diffusion time of $CH_3NH_3PbI_3$ solution. Especially, the tubes protruding from the perovskite film would lead to many undesirable phenomena, such as short circuit and leakage current, of subsequently fabricated devices as shown in Fig. S3. By increasing the loading time before spin-coating, these tubes can then be fully filled by $CH_3NH_3PbI_3$ with an increased perovskite film thickness of around 900 nm (Fig. S1b). However, for the devices with such an active perovskite layer thickness of 900 nm, there would be a significant increase in the series resistance and the mismatch between the perovskite absorption depth and the carrier diffusion length [33]. In this case, the photogenerated carriers typically recombine before reaching the electrodes, since

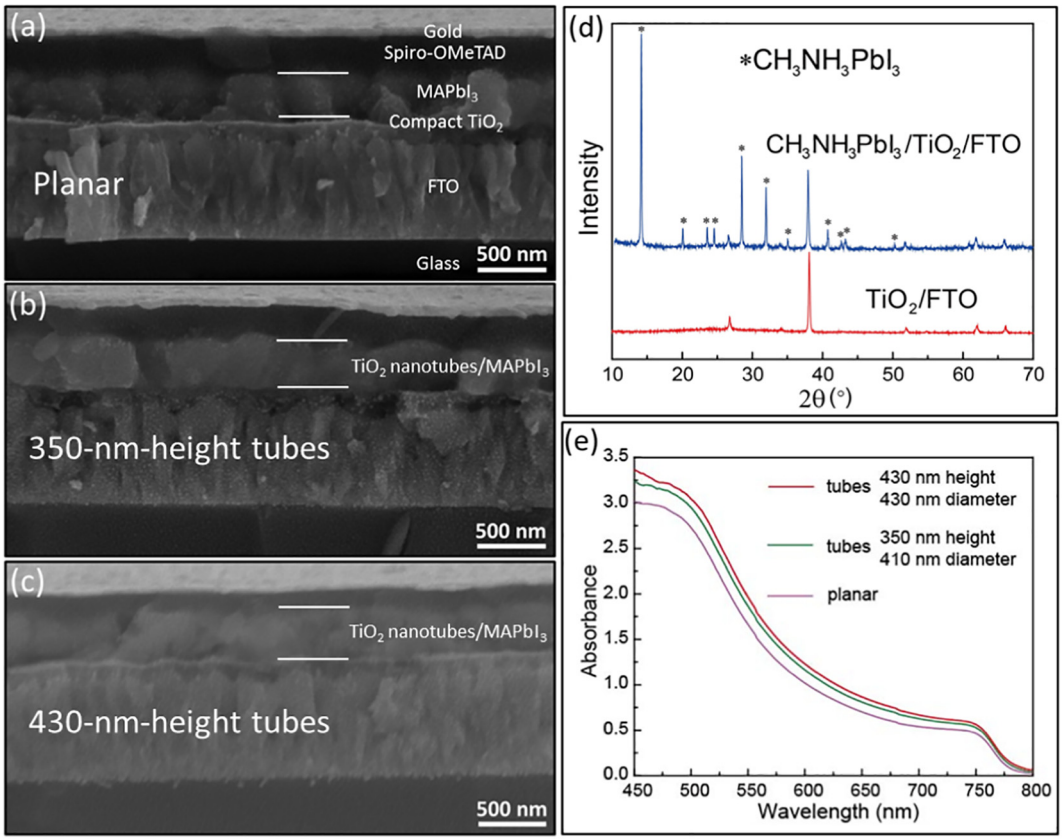

Fig. 3. Cross-sectional SEM images of perovskite solar cells fabricated with $CH_3NH_3PbI_3$ spin-coated on the electrodes of (a) planar, TiO_2 nanotube arrays with the height of (b) 350 nm and (c) 430 nm, respectively. (d) X-ray diffraction (XRD) patterns of TiO_2 nanotubes/c-TiO_2/FTO-coated glass and $CH_3NH_3PbI_3$ deposited on TiO_2 nanotubes/c-TiO_2/FTO-coated glass. (e) UV-vis absorbance of $CH_3NH_3PbI_3$ deposited on both planar and nanotube substrates.

the perovskite layer thickness of 900 nm considerably exceeds the carrier diffusion length of ~100 nm, deteriorating the power conversion efficiency of devices as presented in Fig. S3. Therefore, the devices with the 900-nm-thickness TiO_2 nanotube arrays were not further optimized in this work.

In order to evaluate contact properties between the perovskite crystals and the tube walls, cross-sectional SEM images of the solar cells fabricated with $CH_3NH_3PbI_3$ on both planar c-TiO_2 and TiO_2 nanotube arrayed substrates were first acquired as shown in Fig. 3. In specific, the planar device with the configuration of FTO/c-TiO_2 (50 nm)/perovskite (350 nm)/sipro-OMeTAD (190 nm)/Au (70 nm) demonstrates a dense and smooth perovskite layer (Fig. 3a). Interestingly, for the nanotube arrayed devices, when the perovskite layer thickness increases slightly to 370 nm and 450 nm with the tube height of 350 nm and 430 nm, respectively (Fig. 3b and c), the surface morphology of the perovskite layer is still maintained the same as the one of the planar device. This compact and intact morphology can be achieved on the nanotube arrays with different tube heights because the short tube height is anticipated to prevent the perovskite precursor solution from being zipped away during spin-coating. If the taller tube height is needed, the prolonged loading time can be adopted to ensure the perovskite solution being maintained within the tubes without creating any voids. More importantly, in both cases, the TiO_2 nanotube arrays can be fully and conformally filled with perovskite crystals in which there are not any noticeable cracks and voids observed in the deposited layer. It is therefore reasonable to expect that the as-constructed vertically standing TiO_2 nanotube arrays, with the full filling of high-quality perovskite material, would enhance the light absorption of the active layer and facilitate the efficient electron extraction from perovskite into one-dimensional TiO_2 nanotubes, contributing to the subsequent device performance enhancement. Furthermore, XRD measurements were performed to evaluate crystallinity of the perovskite layer deposited on the 430-nm-height nanotube arrays (Fig. 3d). In addition to the peaks corresponding to the TiO_2/FTO substrate, all the observed diffraction peaks can be ascribed to $CH_3NH_3PbI_3$, indicating excellent crystallinity and high purity of the obtained perovskite layer [30]. It is also worth to mention that during device fabrication, the hole transport material, sipro-OMeTAD, usually requires to undergo a 12 h oxidation treatment to reach the appreciable conductivity [34]. With the purpose to rule out the effect of oxidation on the perovskite layer, the XRD patterns of $CH_3NH_3PbI_3$ with the same oxidation treatment were recorded for comparison (Fig. S4). It is evident that the XRD patterns of perovskite with and without the oxidation treatment are almost identical, demonstrating that the oxidation treatment can hardly cause any change to the perovskite layer.

Apart from that, Fig. 3e compares the absorbance spectra of $CH_3NH_3PbI_3$ deposited on both planar c-TiO_2 and TiO_2 nanotube arrayed substrates. It is shown that $CH_3NH_3PbI_3$ materials exhibit the strong light absorbance in all cases with sharp adsorption edges rising at around 780 nm, further confirming the high-quality of obtained perovskite films. As compared with the planar c-TiO_2 structured substrate, the $CH_3NH_3PbI_3$ deposited on 350-nm-height TiO_2 nanotubes displays the significantly enhanced absorbance over the entire spectrum range. This can be mainly attributed to the stronger light trapping capability of TiO_2 nanotubes as contrasted to that of the planar counterparts [27]. Notably, the absorbance of perovskite layer deposited on 430-nm-height tubes

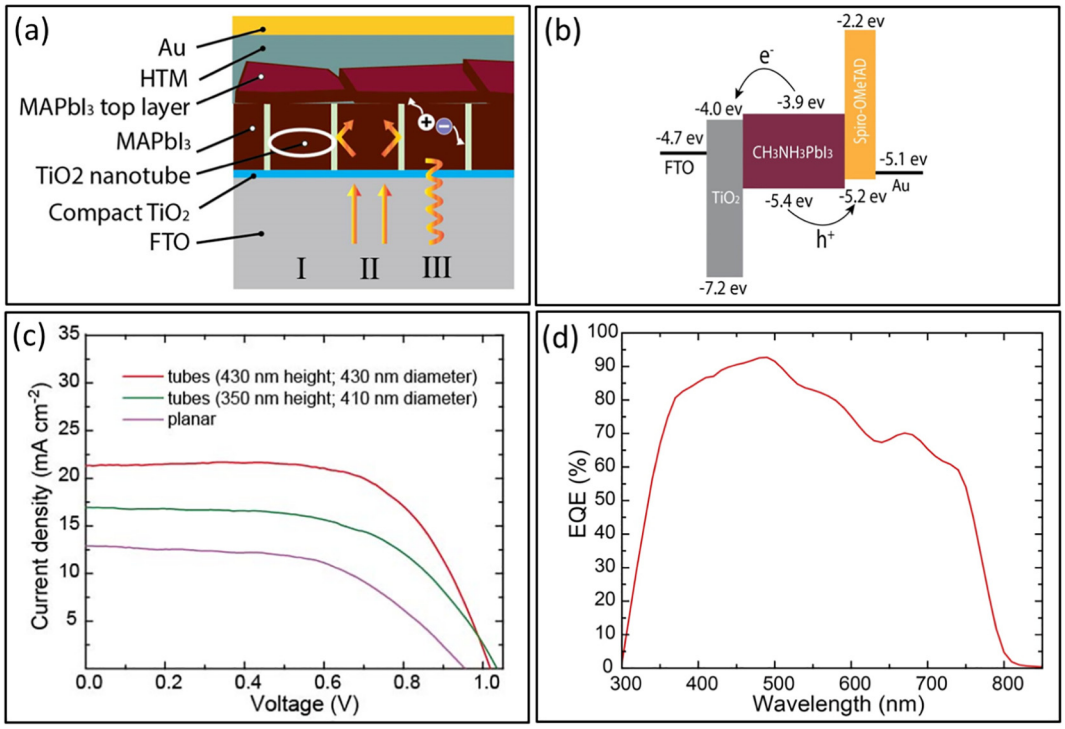

Fig. 4. Device architecture of the perovskite solar cell studied and corresponding equilibrium energy band diagram of the cell. (a) TiO_2 nanotubes-based solar cell architecture with the features of (I) high filling rate, (II) enhanced light-trapping and (III) rapid collection and transport of photoexcited electrons facilitated by the nanotube arrays. (b) Energy levels of various components configured in the device. (c) Current density-voltage (*J-V*) curves of the perovskite devices configured with unoptimized planar and TiO_2 nanotube arrays with the height of 350 nm and 430 nm, respectively. (d) EQE spectrum of the best-performed device with the tube height of 430 nm.

is found to be slightly larger than that of the 350-nm-height tubed substrate, which is mainly derived from the combined effect of enhanced light trapping of higher tubes and thicker perovskite layers. Therefore, these vertical TiO_2 nanotube arrays with the full filling of high-quality perovskite material can be confirmed to enhance the light absorbance and simultaneously facilitate the efficient electron extraction transferring from perovskite to nanotubes in order to improve the corresponding energy conversion efficiency of fabricated devices.

To further elucidate the technological potency of these vertical TiO_2 nanotube arrays as electron transport materials for PVSCs, the devices were fabricated with the typical configuration as depicted in Fig. 4a and their corresponding energy band diagram is shown in Fig. 4b. At first, the photovoltaic performance of devices with both planar c-TiO_2 and 350-nm-height TiO_2 nanotube arrays are compared (Fig. 4c), considering the thickness of the perovskite layer of these devices are almost the same. Evidently, the devices with planar c-TiO_2 exhibit the smaller open-circuit voltage (V_{oc}) of 0.96 V and current density (J_{sc}) of 12.89 mA/cm^2 as compared with the nanotube devices. For a fair comparison, this planar device is not optimized with the device structure, materials and geometry, in which it is purposely fabricated to evaluate and contrast the effect of adopting vertical TiO_2 nanotube arrays in this simple PVSC configuration. In principle, besides the energy band alignment, charge transport and recombination behaviors are the major factors to dictate the V_{oc}. In this case, since there is only one difference occurred at the TiO_2/perovskite interface between the planar and the nanotube devices, we can explicitly reason that the drop in V_{oc} is originated from the limited electron extraction and transport at the c-TiO_2/perovskite interface, which leads to a severe recombination and energy loss within the planar device. Regarding to the decrease in J_{sc}, it can also be well explained by combined effects of the stronger light absorption induced by the enhanced light trapping and the efficient electron extraction/transport of the TiO_2 nanotubes.

Table 1
Photovoltaic performance of perovskite solar cells configured with planar and TiO_2 nanotube arrays.

	J_{sc} (mA/cm^2)	V_{oc} (V)	FF	η (%)
Planar	12.89	0.96	0.54	6.75
350 nm	16.98	1.03	0.58	10.22
430 nm	21.00	1.02	0.66	14.13

In any case, as shown in Fig. 4c and Table 1, the perovskite solar cell configured with 430-nm-height TiO_2 nanotubes shows a champion power conversion efficiency (*PCE*) of 14.13% with a J_{sc} of 21 mA/cm^2, a V_{oc} of 1.02 V and a fill factor (FF) of 0.66. This *PCE* would be considerably dropped to 10.22% for the device fabricated with 350-nm-height TiO_2 nanotubes with a drastically compromised J_{sc} of 16.98 mA/cm^2 and a FF of 0.58. These obvious decreases in J_{sc} and FF can be ascribed to the conceded light trapping and electron collection/transfer capacity induced by the shorter TiO_2 nanotubes. For the vertically standing TiO_2 nanotube arrays with the height of 430 nm, these nanotubes can penetrate into the deeper region of the perovskite layer, and thus forming the highly efficient electron extraction and transfer pathways throughout the entire perovskite layer. Once photo-excited electrons are generated, they will be immediately extracted from the perovskite layer, which significantly eliminates the undesirable electron accumulation and consequently mitigates to the charge recombination. Moreover, the highly oriented one-dimensional electron transport nature of these relatively taller nanotubes (i.e., 430 nm) is beneficial for the overall electron transport. As a result, we can summarize the performance enhancement of adopting TiO_2 nanotubes array in perovskite solar cells as the following, namely (I) high

filling rate, (II) enhanced light-trapping as well as (III) rapid electron collection and transport induced by the tubes as presented in Fig. 4a.

It should also be noted that despite the high *PCE* of 14.13% is achieved under reverse scanning direction in the measured *J-V* characteristic, the device configured with 430-nm-height TiO_2 nanotube arrays demonstrates a relatively anomalous hysteresis there, as shown in Fig. S5. In detail, when the *J-V* curve is recorded under the forward scanning direction, the device shows a decreased *PCE* of 12.92%. This can be attributed to the traps of electrons induced by the defects at the interface between perovskite and TiO_2 nanotubes [35–37]. Interestingly, the spectrum exhibits the much higher EQE in the shorter wavelength region as compared with that measured in the longer wavelength range, further illustrating the efficient carrier extraction and collection at the TiO_2/perovskite interfaces [38]. It is because that the carriers generated by light with the shorter wavelength are more likely to exist in the region close to the TiO_2/perovskite interface due to the limited photon penetration length. Moreover, the integrated J_{sc} is as well determined to be 19.00 mA/cm^2, which is slightly smaller than the J_{sc} value attained in the *J-V* curve (Fig. 4d). Similar phenomena are widely reported in other previous works [39,40].

4. Conclusions

In conclusion, the vertically standing crystalline TiO_2 nanotube arrays with the desired geometry are directly fabricated on the substrate of c-TiO_2/FTO-coated glass and employed as the electron transport material in perovskite solar cells. It is demonstrated that these nanotubes can be fully and conformally filled with perovskite crystals to form a dense and smooth $CH_3NH_3PbI_3$ layer without any pinholes, voids and cracks. Benefiting from the full filling of high-quality perovskite materials, the enhanced light trapping as well as the rapid electron collection and transport induced by one-dimensional TiO_2 nanotube arrays can be realized. As a result, the PVSCs with the optimized tube height can yield a power conversion efficiency (*PCE*) of 14.13%. All these results demonstrate clearly the promising potential of vertical TiO_2 nanotube arrays for PVSCs and other photoelectrochemical applications. In the future, it is expected that the device performance can be further enhanced with the more detailed optimization and precise control of the nanotube arrays geometries such as tube diameters, tube heights, periodicities and so on.

Notes

The authors declare no competing financial interest.

Statement of Authors' contributions

Johnny C. Ho and Xiaoguang Liang conceived and carried out the experiments. Yuanhang Cheng and Sai-Wing Tsang contributed to provide the experimental equipment and the discussion. Xiuwen Xu revised the manuscript. The SEM, XRD and UV-Vis measurements were conducted by Dapan Li, Ziyao Zhou, Guofa Dong and Renjie Wei. Ruoting Dong fabricated the solar cell devices and tested the photovoltaic performance. Johnny C. Ho and Xiaoguang Liang co-wrote the paper.

Acknowledgement

This research was financially supported by the General Research Fund of the Research Grants Council of Hong Kong SAR, China (CityU 11275916)), the National Natural Science Foundation of China (Grants 51672229), the Science Technology and Innovation Committee of Shenzhen Municipality (Grant JCYJ20160229165240684), and was supported by a grant from the Shenzhen Research Institute, City University of Hong Kong.

Appendix A. Supplementary material

SEM images of $CH_3NH_3PbI_3$ films spin-coated on the planar electrode, on the 430-nm-height TiO_2 nanotube arrays with the loading time of 0 s, 15 s, and 30 s, and on the 900-nm-height TiO_2 nanotubes with a loading time of 30 s. *J-V* curves of the perovskite solar cells configured with the 900-nm-height TiO_2 nanotubes measured under reverse scan direction. X-ray diffraction patterns of TiO_2 nanotubes/c-TiO_2/FTO-coated glass, $CH_3NH_3PbI_3$ deposited on TiO_2 nanotubes, as well as $CH_3NH_3PbI_3$ oxidized for 12 hrs. *J-V* curve of the perovskite solar cell fabricated with the 430-nm-height TiO_2 nanotube arrays measured under forward scan direction. Supplementary data associated with this article can be found, in the online version, at https://doi.org/10.1016/j.apsusc.2018.04.245.

References

[1] J. Burschka, N. Pellet, S.J. Moon, R. Humphry-Baker, P. Gao, M.K. Nazeeruddin, M. Gratzel, Sequential deposition as a route to high-performance perovskite-sensitized solar cells, Nature 499 (2013) 316–319.
[2] Q. Dong, Y. Fang, Y. Shao, P. Mulligan, J. Qiu, L. Cao, J. Huang, Electron-hole diffusion lengths >175 μm in solution-grown $CH_3NH_3PbI_3$ single crystals, Science 347 (2015) 967–970.
[3] W.-Y. Rho, H.-S. Kim, W.-J. Chung, J.S. Suh, B.-H. Jun, Y.-B. Hahn, Enhancement of power conversion efficiency with TiO_2 nanoparticles/nanotubes-silver nanoparticles composites in dye-sensitized solar cells, Appl. Surf. Sci. 429 (2018) 23–28.
[4] S.D. Stranks, G.E. Eperon, G. Grancini, C. Menelaou, M.J. Alcocer, T. Leijtens, L.M. Herz, A. Petrozza, H.J. Snaith, Electron-hole diffusion lengths exceeding 1 micrometer in an organometal trihalide perovskite absorber, Science 342 (2013) 341–344.
[5] H. Zhang, J. Mao, H. He, D. Zhang, H.L. Zhu, F. Xie, K.S. Wong, M. Grätzel, W.C.H. Choy, A smooth $CH_3NH_3PbI_3$ film via a new approach for forming the PbI_2 nanostructure together with strategically high CH_3NH_3I concentration for high efficient planar-heterojunction solar cells, Adv. Energy Mater. 5 (2015) 1501354.
[6] X. Xu, C. Ma, Y. Cheng, Y.-M. Xie, X. Yi, B. Gautam, S. Chen, H.-W. Li, C.-S. Lee, F. So, S.-W. Tsang, Ultraviolet-ozone surface modification for non-wetting hole transport materials based inverted planar perovskite solar cells with efficiency exceeding 18%, J. Power Sources 360 (2017) 157–165.
[7] Y. Cheng, H.-W. Li, J. Zhang, Q.-D. Yang, T. Liu, Z. Guan, J. Qing, C.-S. Lee, S.-W. Tsang, Spectroscopic study on the impact of methylammonium iodide loading time on the electronic properties in perovskite thin films, J. Mater. Chem. A 4 (2016) 561–567.
[8] M.-C. Wu, W.-C. Chen, S.-H. Chan, W.-F. Su, The effect of strontium and barium doping on perovskite-structured energy materials for photovoltaic applications, Appl. Surf. Sci. (2017) 9–15.
[9] H.K. Adli, T. Harada, W. Septina, S. Hozan, S. Ito, S. Ikeda, Effects of porosity and amount of surface hydroxyl groups of a porous TiO_2 layer on the performance of a $CH_3NH_3PbI_3$ perovskite photovoltaic cell, J. Phys. Chem. C 119 (2015) 22304–22309.
[10] W.S. Yang, B.-W. Park, E.H. Jung, N.J. Jeon, Y.C. Kim, D.U. Lee, S.S. Shin, J. Seo, E. K. Kim, J.H. Noh, Iodide management in formamidinium-lead-halide–based perovskite layers for efficient solar cells, Science 356 (2017) 1376–1379.
[11] F. Bella, C. Gerbaldi, C. Barolo, M. Gratzel, Aqueous dye-sensitized solar cells, Chem. Soc. Rev. 44 (2015) 3431–3473.
[12] A. El Ruby Mohamed, S. Rohani, Modified TiO_2 nanotube arrays (TNTAs): progressive strategies towards visible light responsive photoanode, a review, Energy Environ. Sci. 4 (2011) 1065.
[13] K. Zhu, N.R. Neale, A. Miedaner, A.J. Frank, Enhanced charge-collection efficiencies and light scattering in dye-sensitized solar cells using oriented TiO_2 nanotubes arrays, Nano Lett. 7 (2007) 69–74.
[14] D. Zhong, B. Cai, X. Wang, Z. Yang, Y. Xing, S. Miao, W.-H. Zhang, C. Li, Synthesis of oriented TiO_2 nanocones with fast charge transfer for perovskite solar cells, Nano Energy 11 (2015) 409–418.
[15] K. Mahmood, B.S. Swain, A. Amassian, Highly efficient hybrid photovoltaics based on hyperbranched three-dimensional tio$_2$ electron transporting materials, Adv. Mater. 27 (2015) 2859–2865.
[16] A. Fakharuddin, F. Di Giacomo, A.L. Palma, F. Matteocci, I. Ahmed, S. Razza, A. D'Epifanio, S. Licoccia, J. Ismail, A. Di Carlo, Vertical TiO_2 nanorods as a medium for stable and high-efficiency perovskite solar modules, ACS Nano 9 (2015) 8420–8429.
[17] H.S. Kim, J.W. Lee, N. Yantara, P.P. Boix, S.A. Kulkarni, S. Mhaisalkar, M. Gratzel, N.G. Park, High efficiency solid-state sensitized solar cell-based on

submicrometer rutile TiO_2 nanorod and $CH_3NH_3PbI_3$ perovskite sensitizer, Nano Lett. 13 (2013) 2412–2417.
[18] K. Mahmood, B.S. Swain, A.R. Kirmani, A. Amassian, Highly efficient perovskite solar cells based on a nanostructured WO_3–TiO_2 core–shell electron transporting material, J. Mater. Chem. A 3 (2015) 9051–9057.
[19] F. Xiao, Layer-by-layer self-assembly construction of highly ordered metal-TiO_2 nanotube arrays heterostructures (M/TNTs, M = Au, Ag, Pt) with tunable catalytic activities, J. Phys. Chem. C 116 (2012) 16487–16498.
[20] Y. Lan, X. Gao, H. Zhu, Z. Zheng, T. Yan, F. Wu, S.P. Ringer, D. Song, Titanate nanotubes and nanorods prepared from rutile powder, Adv. Funct. Mater. 15 (2005) 1310–1318.
[21] M.S. Sander, M.J. Côté, W. Gu, B.M. Kile, C.P. Tripp, Template-assisted fabrication of dense, aligned arrays of titania nanotubes with well-controlled dimensions on substrates, Adv. Mater. 16 (2004) 2052–2057.
[22] X. Gao, J. Li, S. Gollon, M. Qiu, D. Guan, X. Guo, J. Chen, C. Yuan, A TiO_2 nanotube network electron transport layer for high efficiency perovskite solar cells, Phys. Chem. Chem. Phys. 19 (2017) 4956–4961.
[23] X. Gao, J. Li, J. Baker, Y. Hou, D. Guan, J. Chen, C. Yuan, Enhanced photovoltaic performance of perovskite $CH_3NH_3PbI_3$ solar cells with freestanding TiO_2 nanotube array films, Chem. Commun. (Camb.) 50 (2014) 6368–6371.
[24] R. Salazar, M. Altomare, K. Lee, J. Tripathy, R. Kirchgeorg, N.T. Nguyen, M. Mokhtar, A. Alshehri, S.A. Al-Thabaiti, P. Schmuki, Use of anodic TiO_2 nanotube layers as mesoporous scaffolds for fabricating $CH_3NH_3PbI_3$ perovskite-based solid-state solar cells, ChemElectroChem 2 (2015) 824–828.
[25] X. Wang, Z. Li, W. Xu, S.A. Kulkarni, S.K. Batabyal, S. Zhang, A. Cao, L.H. Wong, TiO_2 nanotube arrays based flexible perovskite solar cells with transparent carbon nanotube electrode, Nano Energy 11 (2015) 728–735.
[26] J. Zhang, T. Pauporte, One-dimesional self-standing TiO_2 nanotube array layers designed for perovskite solar cell applications, Chemphyschem (2015) 2836–2841.
[27] X. Liang, H. Zhang, H.W. Li, L. Shu, H. Cheung, D. Li, S. Yip, Q.D. Yang, C.Y. Wong, S.W. Tsang, J.C. Ho, Enhanced self-assembly of crystalline, large-area, and periodicity-tunable TiO_2 nanotube arrays on various substrates, ACS Appl. Mater. Interfaces 9 (2017) 6265–6272.
[28] M. Fang, H. Lin, H.Y. Cheung, S. Yip, F. Xiu, C.Y. Wong, J.C. Ho, Optical nanoscale patterning through surface-textured polymer films, Adv. Opt. Mater. 2 (2014) 855–860.
[29] M. Fang, H. Lin, H.Y. Cheung, F. Xiu, L. Shen, S. Yip, E.Y. Pun, C.Y. Wong, J.C. Ho, Polymer-confined colloidal monolayer: a reusable soft photomask for rapid wafer-scale nanopatterning, ACS Appl. Mater. Interfaces 6 (2014) 20837–20841.
[30] N. Ahn, D.Y. Son, I.H. Jang, S.M. Kang, M. Choi, N.G. Park, Highly reproducible perovskite solar cells with average efficiency of 18.3% and best efficiency of 19.7% fabricated via lewis base adduct of lead(II) iodide, J. Am. Chem. Soc. 137 (2015) 8696–8699.
[31] M. Xiao, F. Huang, W. Huang, Y. Dkhissi, Y. Zhu, J. Etheridge, A. Gray-Weale, U. Bach, Y.B. Cheng, L. Spiccia, A fast deposition-crystallization procedure for highly efficient lead iodide perovskite thin-film solar cells, Angew. Chem. Int. Ed. Engl. 53 (2014) 9898–9903.
[32] W. Wu, A. Katsnelson, O.G. Memis, H. Mohseni, A deep sub-wavelength process for the formation of highly uniform arrays of nanoholes and nanopillars, Nanotechnology 18 (2007) 485302.
[33] D. Liu, M.K. Gangishetty, T.L. Kelly, Effect of $CH_3NH_3PbI_3$ thickness on device efficiency in planar heterojunction perovskite solar cells, J. Mater. Chem. A 2 (2014) 19873–19881.
[34] W.H. Nguyen, C.D. Bailie, E.L. Unger, M.D. McGehee, Enhancing the hole-conductivity of spiro-OMeTAD without oxygen or lithium salts by using spiro $(TFSI)_2$ in perovskite and dye-sensitized solar cells, J. Am. Chem. Soc. 136 (2014) 10996–11001.
[35] E.L. Unger, E.T. Hoke, C.D. Bailie, W.H. Nguyen, A.R. Bowring, T. Heumüller, M. G. Christoforo, M.D. McGehee, Hysteresis and transient behavior in current–voltage measurements of hybrid-perovskite absorber solar cells, Energy Environ. Sci. 7 (2014) 3690–3698.
[36] H.J. Snaith, A. Abate, J.M. Ball, G.E. Eperon, T. Leijtens, N.K. Noel, S.D. Stranks, J. T. Wang, K. Wojciechowski, W. Zhang, Anomalous hysteresis in perovskite solar cells, J. Phys. Chem. Lett. 5 (2014) 1511–1515.
[37] H.S. Kim, I. Mora-Sero, V. Gonzalez-Pedro, F. Fabregat-Santiago, E.J. Juarez-Perez, N.G. Park, J. Bisquert, Mechanism of carrier accumulation in perovskite thin-absorber solar cells, Nat. Commun. 4 (2013) 2242.
[38] C. Bi, X. Zheng, B. Chen, H. Wei, J. Huang, Spontaneous passivation of hybrid perovskite by sodium ions from glass substrates: mysterious enhancement of device efficiency revealed, ACS Energy Lett. 2 (2017) 1400–1406.
[39] Y. Chen, Y. Sun, J. Peng, W. Zhang, X. Su, K. Zheng, T. Pullerits, Z. Liang, Tailoring organic cation of 2D air-stable organometal halide perovskites for highly efficient planar solar cells, Adv. Energy Mater. 7 (2017) 1700162.
[40] J. Peng, Y. Chen, X. Zhang, A. Dong, Z. Lian, g Solid-state ligand-exchange fabrication of $CH_3NH_3PbI_3$ capped PbS quantum dot solar cells, Adv Sci (Weinh) 3 (2016) 1500432.